Compact 20-pass thin-disk multipass amplifier stable against thermal lensing effects and delivering 330 mJ pulses with $M^2 < 1.17$

Manuel Zeyen, Lukas Affolter, Marwan Abdou Ahmed, Thomas Graf, Oguzhan Kara, Klaus Kirch, Miroslaw Marszalek, François Nez, Ahmed Ouf, Randolf Pohl, et al.

Research Article Vol. 32, No. 2 / 15 Jan 2024 / Optics Express 1218
Optics EXPRESS

Compact 20-pass thin-disk multipass amplifier stable against thermal lensing effects and delivering 330 mJ pulses with $M^2 < 1.17$

MANUEL ZEYEN,[1] LUKAS AFFOLTER,[1] MARWAN ABDOU AHMED,[2] THOMAS GRAF,[2] OGUZHAN KARA,[1,3] KLAUS KIRCH,[1,3] MIROSLAW MARSZALEK,[1,3] FRANÇOIS NEZ,[4] AHMED OUF,[5] RANDOLF POHL,[5,6] IVO SCHULTHESS,[1] SIDDHARTH RAJAMOHANAN,[5] PAULINE YZOMBARD,[4] KARSTEN SCHUHMANN,[1] AND ALDO ANTOGNINI[1,3,*]

[1]*Institute for Particle Physics and Astrophysics,ETH Zurich, 8093 Zurich, Switzerland*
[2]*Institut für Strahlwerkzeuge, Universität Stuttgart, Pfaffenwaldring 43, 70569 Stuttgart, Deutschland, Germany*
[3]*Laboratory for Particle Physics, Paul Scherrer Institute, 5232 Villigen, Switzerland*
[4]*Laboratoire Kastler Brossel, Sorbonne Université, CNRS, ENS-Université PSL, Collège de France, 75252 Paris Cedex 05, France*
[5]*QUANTUM, Institute of Physics, Johannes Gutenberg-Universität Mainz, 55099 Mainz, Germany*
[6]*Excellence Cluster PRISMA+, Johannes Gutenberg-Universität Mainz, 55099 Mainz, Germany*
[*]*aldo.antognini@psi.ch*

Abstract: We report on an Yb:YAG thin-disk multipass amplifier delivering 100 ns long pulses at a central wavelength of 1030 nm with an energy of 330 mJ at a repetition rate of 100 Hz. The beam quality factor at the maximum energy was measured to be $M^2 < 1.17$. The small signal gain is 21.7, and the gain at 330 mJ was measured to be 6.9. The 20-pass amplifier is designed as a concatenation of stable resonator segments in which the beam is alternately Fourier transformed and relay-imaged back to the disk by a 4f-imaging optical scheme stage. The Fourier transform propagation makes the output beam robust against spherical phase front distortions, while the 4f-stage is used to compensate the thermal lens of the thin-disk and to reduce the footprint of the amplifier.

1. Introduction

Multipass amplifiers are versatile tools for the generation of high-power and high-energy laser beams. Systems delivering kWs of average power have been demonstrated at all pulse lengths from continuous wave down to femtoseconds. In particular, thin-disk (TD) multipass amplifiers have shown their great potential in combining high power/energy output with diffraction limited beam quality and high flexibility regarding the input pulse length [1–3]. While TD regenerative amplifiers delivering excellent beam quality at kW average power have been demonstrated [4], TD multipass amplifiers have distinct properties which can be advantageous compared to a regenerative amplifier. As shown in Fig. 1, TD multipass amplifiers, are very flexible with respect to the repetition rate (few tens of Hz up to few GHz [5]) in comparison to TD regenerative amplifiers, which are typically limited by the Pockels cell drivers to approximately 1 MHz. Furthermore, scaling the average power of a TD regenerative amplifier to the kW or even multi-kW output power level requires a highly stable resonator design, which can be challenging to achieve because of the rise of thermally induced aberrations at high pump power densities. In the case of a TD multipass amplifier this is less of a challenge. While both types of systems

#506962 https://doi.org/10.1364/OE.506962
Journal © 2024 Received 27 Sep 2023; revised 8 Nov 2023; accepted 9 Nov 2023; published 2 Jan 2024

Optics EXPRESS

have their merits, one could argue for a TD multipass amplifier with optimized disk parameters (like the one presented here) as a powerful booster for a TD regenerative system, to target pulse energies at the Joule level.

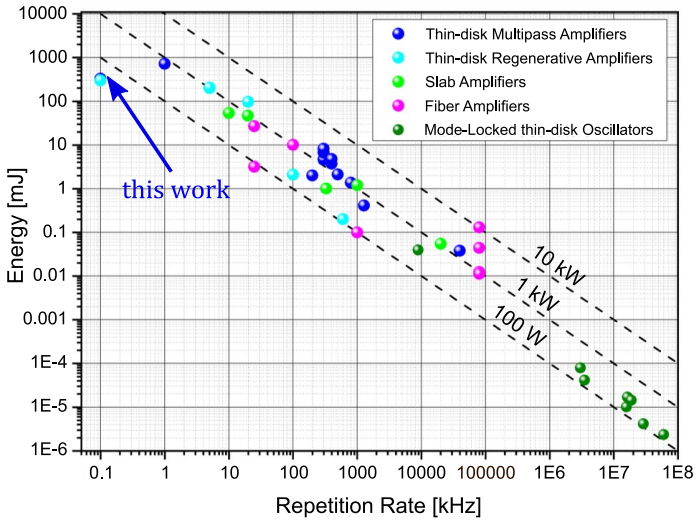

Fig. 1. Selected overview of achieved output pulse energy of thin-disk multipass, and thin-disk regenerative amplifier systems versus output pulse repetition rate. For comparison, results for slab and fiber amplifiers as well as mode-locked thin-disk oscillators are added.

High-energy applications benefiting from good beam quality are numerous, and include for example large area material texturing, parallel material processing via diffractive optical elements (DOEs), or large area ablations processes. For more examples see [6] (and references therein). Note, that while many microprocessing applications require high-energy ultrashort pulses, some applications like direct laser interference patterning (DLIP) especially benefit from high-energy nanosecond pulses as the processing region can be made larger compared to when ultrashort pulses are used.

Most thin-disk multipass amplifier designs are based on three main categories: relay-imaging (4f-imaging) [7–12], quasi-collimated propagation (QC, or lens guide) [13–17] or resonator-based optical Fourier transform (FT) propagations [18–20]. In 4f-based designs, the beam is imaged from active medium (AM) to active medium so that its size remains constant for each pass (if soft aperture effects are neglected). These systems are relatively compact and input beams with a wide variety of beam parameters can be propagated. However, phase front distortions introduced by thermal effects in the AM add up with each pass over the AM, limiting the achievable beam quality and stability of such an amplifier. In the QC design the beam propagates almost freely in the amplifier. Only weakly focusing elements are used to compensate the beam divergence and ensure the same size of the beam on each pass over the AM. This type of multipass amplifier is relatively convenient to set up and has the additional advantage that the propagating beam stays large along the whole propagation path, which makes the QC scheme an excellent choice for the highest power applications with excellent beam quality [21]. While this design is less sensitive to phase front distortions at the AM than the 4f-design, a third design based on FT propagations provides the highest stability against both spherical and aspherical phase front distortions [22,23].

The FT design can be understood as an unfolded FT resonator of a corresponding regenerative amplifier. The amplifier thus inherits the stability of the FT resonator w.r.t. thermal lensing so that FT-based multipass amplifiers have the potential to deliver near diffraction limited output beams at kW (Joule) level output power (energy). However, a resonator-based multipass amplifier

Optics EXPRESS

typically requires careful setup and mode matching of the input beam to the resonator mode, and a rather large mirror array.

Here we report on the development of a multipass amplifier that combines the advantages of the 4f-based imaging approach with the stability of the FT-resonator design. This hybrid amplifier is part of the laser system of the HyperMu experiment, in which the CREMA (Charge Radius Experiments with Muonic Atoms) collaboration aims at measuring the ground-state hyperfine splitting of muonic hydrogen [24,25]. In this system a single-frequency Yb:YAG thin-disk laser (TDL), composed of an oscillator followed by the here presented amplifier, is used for pumping mid-IR optical parametric oscillators (OPOs) and optical parametric amplifiers (OPAs). The input laser pulses to the amplifier are provided by an injection seeded TDL oscillator which is frequency stabilized via the Pound-Drever-Hall method [26,27]. The TDL oscillator delivers single-frequency pulses of up to 50 mJ energy and a pulse length between 50-100 ns with nearly diffraction limited beam quality. Ultimately, the goal is to develop an amplifier which delivers nanoseconds pulses with 500 mJ of pulse energy and an excellent beam quality factor together with a very high long-term energy/power and pointing stability.

In the following, Section 2 introduces the multipass amplifier concept, and Section 3 further elaborates on the optical layout. In Section 4, we describe the experimental realization of our hybrid multipass amplifier and discusses the advantages of including a 4f-stage in the propagation scheme. Finally the experimental results are presented in Section 5.

2. Amplifier concept

The amplifier architecture includes a double 4f-imaging stage and an optical Fourier transform (FT) segment, so that the propagation follows the sequence

$$4f - \text{ disk } - \text{FT} - \text{ disk } - 4f - 4f - \text{ disk } - \text{FT} - \text{ disk } \cdots, \tag{1}$$

where the disk forms the beginning and the end of the FT propagation. Neglecting thermal lensing and aperture effects in the disk, the ABCD matrix of the basic double-pass segment $4f$ – disk – FT – disk – $4f$ is conveniently given by

$$M = M_{4\text{f}} M_{\text{FT}} M_{4\text{f}} = \begin{pmatrix} -1 & 0 \\ 0 & -1 \end{pmatrix} \begin{pmatrix} 0 & F \\ -\frac{1}{F} & 0 \end{pmatrix} \begin{pmatrix} -1 & 0 \\ 0 & -1 \end{pmatrix} = \begin{pmatrix} 0 & F \\ -\frac{1}{F} & 0 \end{pmatrix}, \tag{2}$$

where F is the so-called Fourier parameter [22,23]. Only a collimated input beam with a radius ($1/e^2$) of

$$w_0 = \sqrt{\frac{\lambda F}{\pi}} \tag{3}$$

is reproduced by the ABCD matrix (2) of this double-pass segment. In general, this makes resonator-based multipass amplifiers less flexible compared to 4f-based designs.

However, the advantage of the FT-resonator based approach becomes apparent when the disk's focal power (i.e., inverse focal length) changes by a small amount ΔV, e.g. due to thermal lensing or variations of is curvature in the manufacturing process. Indeed, the FT propagation stabilizes the output beam parameters (size and phase front curvature) against ΔV. After a single round-trip through a double-pass segment, the sensitivity of the output beam parameters to ΔV is small, and given by [22]

$$\frac{w_{\text{out}}(\Delta V)}{w_0} = 1 + \frac{1}{2} F^2 \Delta V^2 - \frac{1}{8} F^4 \Delta V^4 + \ldots, \tag{4}$$

$$\frac{1}{R_{\text{out}}(\Delta V)} = -F^2 \Delta V^3 + F^4 \Delta V^5 - \ldots, \tag{5}$$

Optics EXPRESS

where F is given by Eq. (3). For a 20-pass amplifier, as used in this study, the sensitivity of the output beam parameters is

$$\frac{w_{20\text{-pass}}(\Delta V)}{w_0} = 1 + 50F^4\Delta V^4 + \ldots, \tag{6}$$

$$\frac{1}{R_{20\text{-pass}}(\Delta V)} = 10F^2\Delta V^3 + \ldots. \tag{7}$$

As illustrated in Fig. 2, the beam parameters change only marginally for small ΔV (in the stability zone), and the width of this stability zone is independent of the number of passes, contrary to the 4f-based design [18,22]. As visible in Fig. 3 the width of the stability zone strongly depends on w_0 which is a consequence of the design of the FT multipass amplifier as a resonator. Nevertheless, as shown in Fig. 4, the stability zone is still noticeable in contrast to purely QC or 4f-based designs [23,28].

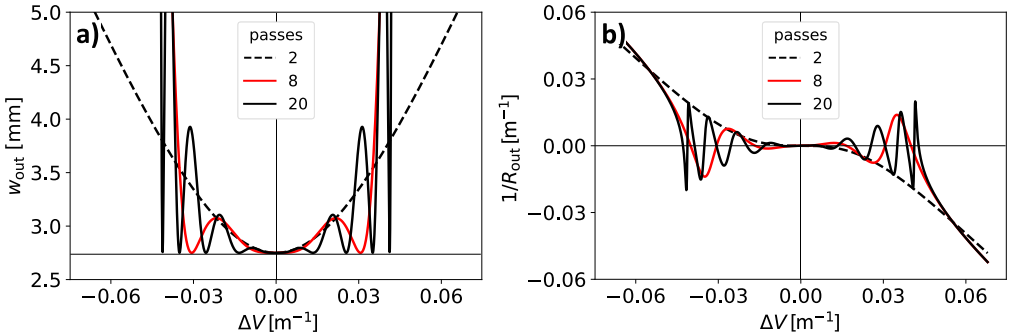

Fig. 2. Variation of the output beam size **a)** and phase front curvature **b)** against changes ΔV in the focal power of the disk for 2-, 8- and 20-passes on the disk in our hybrid-amplifier. The Fourier propagation of the amplifier was setup to accomodate an input beam of waist w_0 = 2.75 mm, corresponding to F = 23.1 m.

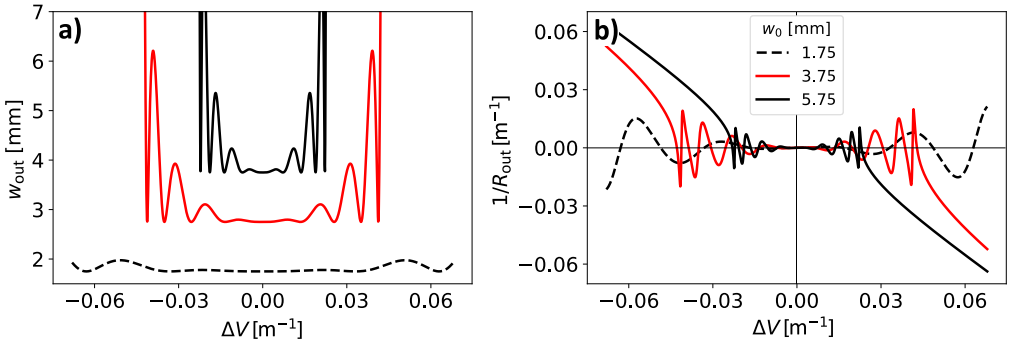

Fig. 3. Variation of the output beam size **a)** and phase front curvature **b)** against changes ΔV in the focal power of the disk for various beam sizes in a 20-pass hybrid-amplifier with w_0 = 1.75, 2.75 and 3.75 mm, corresponding to F = 9.3, 23.1 and 42.9 m, respectively.

The stability against small changes of the focal power of the disk and the suppression of higher order aberrations by the FT and the soft aperture at the disk not only make long-term operation of the amplifier robust but also simplify commissioning of the system (the amplifier can be initially setup at zero pump load and the beam shape always remains Gaussian).

Optics EXPRESS

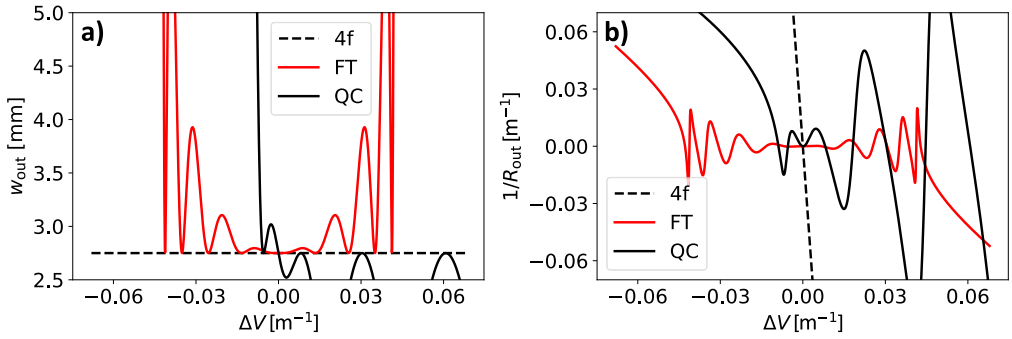

Fig. 4. Variation of the output beam size **a)** and phase front curvature **b)** against changes ΔV in the focal power of the disk for 20-passes in a quasi-collimated (QC), a 4f-based and a FT-based multipass amplifier.

3. Optical layout

In practice, it is crucial to shorten the FT propagation by realizing it as a Galilean telescope [22]. Such a telescope can be realized by a concave-shaped disk and a convex-shaped mirror, with the FT being performed over a round-trip through the telescope, i.e., from just before the disk back to just after the disk. The layout of the telescope is then calculated by matching the Galilean telescope to the ABCD matrix given in Eq. (2). A realization of such an amplifier is shown in Fig. 5 where the separation d_1 between the disk and the convex mirror and the separation d_2 between the convex mirror and the end mirror are given by [23]

$$d_1 = f_{\text{vex}} + f_{\text{D}} \frac{F}{F - f_{\text{D}}}, \tag{8}$$

$$d_2 = f_{\text{vex}} + \frac{1}{2}\left(\frac{f_{\text{vex}}}{f_{\text{D}}}\right)^2 F - \frac{f_{\text{vex}}^2}{2F}, \tag{9}$$

where f_{D} is the disk's focal length, and f_{vex} is the focal length of the convex mirror. The beam waist w_2 on the end-mirror M_2 is given by

$$w_2 = \frac{\sqrt{2}}{2} w_0 f_{\text{vex}} \left(\frac{1}{F} - \frac{1}{f_{\text{D}}}\right), \tag{10}$$

which serves to evaluate potential issues related to laser-induced damage. While it is typically advantageous to realise the Galilean telescope in the FT branch with a curved disk, we had to use flat disks. Indeed, to maximize the extractable energy from the disk, i.e., to minimize amplified spontaneous emission effects, we used a rather thick and low-doped disk (600 µm, 2.3 at.%) [23]. It turned out to be problematic to contact such disks on curved diamond heat-spreaders so we contacted the disk on a flat diamond (1.9 mm thickness). The resulting focal length of the disk was $f_{\text{D}} \approx 10$ m, which is too large for a standard Galilean telescope setup. However, if the 4f-stage is detuned, i.e., the separation between the focusing elements is changed from $2f$ to $2f + \delta$, an effective lens is produced at the disk. Indeed, the ABCD matrix of such a detuned 4f-stage is given by [29]

$$M_{4\text{f}}(\delta) = \begin{pmatrix} 1 & f \\ 0 & 1 \end{pmatrix} \begin{pmatrix} 1 & 0 \\ -\frac{1}{f} & 1 \end{pmatrix} \begin{pmatrix} 1 & 2f+\delta \\ 0 & 1 \end{pmatrix} \begin{pmatrix} 1 & 0 \\ -\frac{1}{f} & 1 \end{pmatrix} \begin{pmatrix} 1 & f \\ 0 & 1 \end{pmatrix} = \begin{pmatrix} -1 & 0 \\ \frac{\delta}{f^2} & -1 \end{pmatrix}, \tag{11}$$

which is equivalent to a 4f-stage followed by a thin lens of focal length $f' = f^2/\delta$. Placing the disk directly after the detuned 4f-stage thus allows to tune the disk's effective focal length. With

Optics EXPRESS

a detuned 4f-stage, Eq. (8) and Eq. (9) are still valid when replacing

$$\frac{1}{f_{\mathrm{D}}} \rightarrow \frac{1}{f_{\mathrm{eff}}} = \frac{1}{f_{\mathrm{D}}} + \frac{1}{f'}. \tag{12}$$

The output beam parameters are again stable against variations of ΔV since the round-trip ABCD matrix still has the form given by (2).

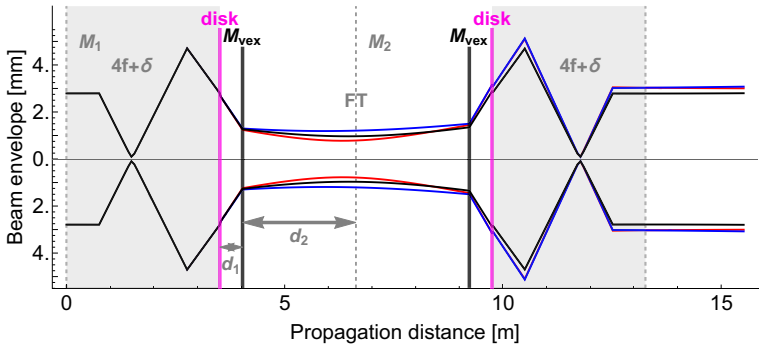

Fig. 5. Beam envelope ($1/e^2$ intensity-radius) in the basic double-pass segment of our hybrid amplifier with a detuned 4f-stage. The input beam has a waist of 2.75 mm. The location of the disk is shown in magenta. The black line indicates the beam size for a disk with nominal focal power, i.e., $\Delta V = 0$. The red and blue lines are propagations for $\Delta V = \pm 0.01\ \mathrm{m}^{-1}$.

During operation, the effective lens introduced by the 4f-stage can also be employed to compensate for deviations of the focal power of the disk from its design value (e.g. due to thermal lensing under high pump load or manufacturing uncertainties) [23,30]. The detuning $\delta = \delta_{\mathrm{D}} + \delta_{\mathrm{V}}$ can be split into two parts: a fixed part

$$\delta_{\mathrm{D}} = f^2 \left(\frac{1}{f'} - \frac{1}{f_{\mathrm{D}}} \right), \tag{13}$$

used to set f_{eff} to realize the nominal design, and a variable part

$$\delta_{\mathrm{V}} = -f^2 \Delta V \tag{14}$$

used to compensate for uncertain ΔV. Operation in the center of the stability zone of the amplifier can be achieved by fine tuning δ, resulting in optimal stability of the output beam parameters against thermal lensing.

Figure 5 shows the calculated beam size in the basic double-pass segment of our hybrid amplifier. While the black curves indicate the beam size for a disk with nominal focal power $1/f_{\mathrm{D}} \approx 0.01\ \mathrm{m}^{-1}$ (i.e., about 10 m focal length), the red and blue curves illustrate the situation where the disk's focal power was changed by $\Delta V = \pm 0.02\ \mathrm{m}^{-1}$, respectively.

The 4f-stage is realized with two concave mirrors of focal length $f = 0.75$ m. The separation between the two concave mirrors was increased by $\delta = 0.515$ m to yield $f_{\mathrm{eff}} \approx 1.5$ m. The FT propagation was designed to keep the beam radius ($1/e^2$) on the disk at $w_0 = 2.75$ mm while preserving a large enough waist $w_2 \approx 0.8$ mm on the end-mirror M_2. The convex mirror used in the Galilean telescope of the FT branch has focal length $f_{\mathrm{vex}} = -0.5$ m. Inserting these numbers into Eq. (8) and Eq. (9) yields $d_1 = 0.52$ m and $d_2 = 2.6$ m, respectively.

Figure 6 shows the calculated beam size along the whole 20-pass amplifier. The comparison between the various curves (defined as in Fig. 5) demonstrates that the beam size at the disk as well as the output beam size and its divergence are insensitive to changes of the disk's focal

Optics EXPRESS

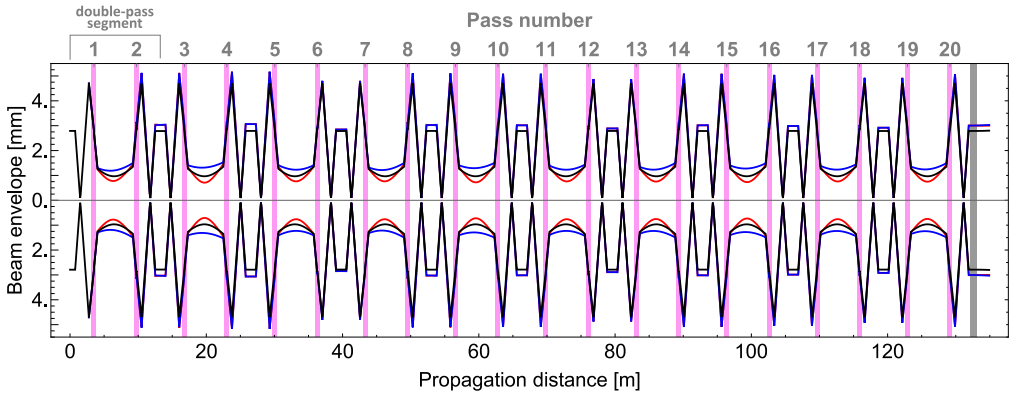

Fig. 6. Beam envelope in our 20-pass hybrid amplifier. The location of the disk is shown in magenta. The black line indicates the beam size for a disk with nominal focal power, i.e., $\Delta V = 0$. The red and blue lines are propagations for $\Delta V = \pm 0.01\ \mathrm{m}^{-1}$.

power ΔV. This stability provided by the FT part of the propagation in our hybrid multipass amplifier allows large beam sizes on the disk.

Moreover, this amplifier architecture allows to design a large mode size throughout the FT propagation which is a needed property for energy scaling. Assuming practical values for $d_1 \in [0.5\,\mathrm{m}, 1.5\,\mathrm{m}]$ and $d_2 \in [1.5\,\mathrm{m}, 3\,\mathrm{m}]$, the beam waist on the end mirrors w_2 can be designed to take any value between 0.5 mm and 1.5 mm (using Eqs. 10) and (14)), demonstrating the flexibility and energy scalability of the system. When doing so, f_{vex} and δ must be chosen appropriately.

4. Experimental realization

Figure 7 shows a schematic of the realized amplifier. The input beam is linearly polarized, has a beam quality of M^2<1.1 and a $1/e^2$ radius of 2.75 mm [27]. It is injected into the amplifier through a thin-film polarizer (TFP) and relay imaged to the disk via the 4f-stage (consisting of $M_{\mathrm{cav,\,1}}$ and $M_{\mathrm{cav,\,2}}$ separated by two plane folding mirrors $M_{\mathrm{plan,\,1}}$ and $M_{\mathrm{plan,\,1}}$). The beam then enters the FT part of the amplifier where it is guided from the disk, via the convex mirror M_{vex} and a folding mirror, to array mirror 1. From there, the beam is directed to end-mirror $M_{2,1}$ which is equipped with a quarter-wave plate that ensures 90° rotation of the polarization after the double pass. Upon reflection again at the disk, the beam has undergone a Fourier transform (i.e., the profile of the beam leaving the disk corresponds to the FT of the beam impinging for the first time on the disk). Since the polarization was rotated, the beam is now imaged to end-mirror M_1 undergoing a reflection at the TFP. In the following round trips, the 4f-stage allows angular multiplexing on the disk similar to the multipass TDL oscillator presented in [29]. Thus, a second mirror array in the 4f branch of the amplifier is not required. The small angular spread of the beams on the disk is amplified by M_{vex}. The mirror array sends the beam alternately to $M_{2,2}$ and $M_{2,3}$ and the beam is kept circulating in the amplifier by reflecting at the TFP. On the final pass, the beam is sent over $M_{2,4}$, which is also equipped with a quarter-wave plate. In a double-pass through this wave plate, the polarization of the beam is rotated back so that the beam is transmitted by the TFP and exits the amplifier. Since $M_{2,1}$ and $M_{2,4}$ are separated vertically, the in- and out-going beams propagate under different angles and can easily be separated. The propagation scheme over the mirror array and the end-mirrors is sketched in the inset of Fig. 7.

While purely FT based amplifier designs are well known to deliver high-quality beams [19,31], the addition of a 4f-stage to such a multipass amplifier is new and provides several advantages. For example, as mentioned, our multipass amplifier design requires on average only one array

Optics EXPRESS

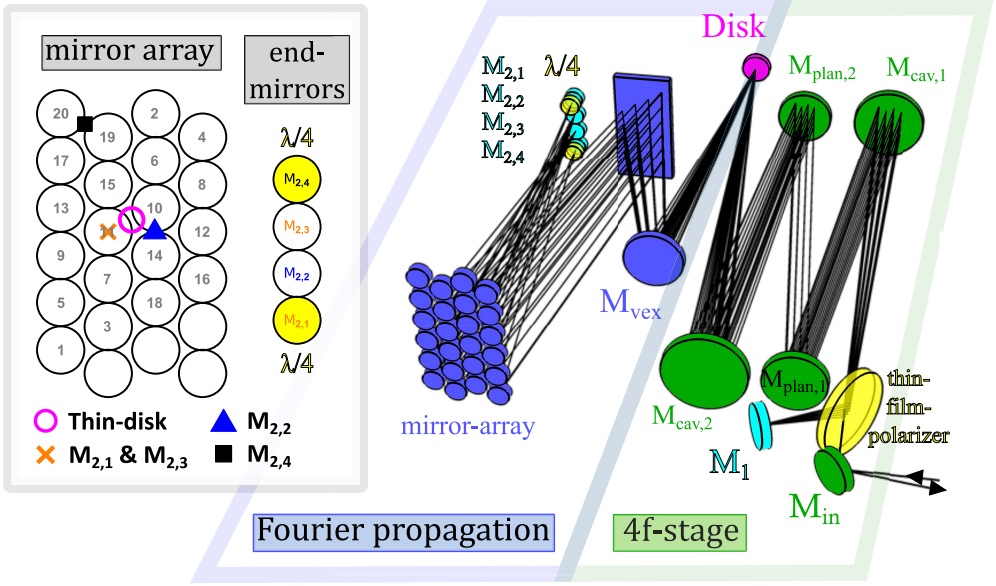

Fig. 7. Schematic of the hybrid 20-pass amplifier. The footprint is 0.4 m × 1 m. Color coding: Disk – magenta, 4f-stage – green, Fourier propagation – blue, end-mirrors – cyan, thin film polarizer and wave plates – yellow. Inset: Mirror array with the mirrors numbered in order of use. The symbols indicate where the symmetry axis of the corresponding optical element intersects the plane of the mirror array. All four locations act as point reflectors leading to the indicated propagation sequence. The yellow shaded mirrors of the end-mirror array have a quarter-wave plate placed in front of them.

mirror per pass over the disk thanks to the 4f-stage. This is half the number of mirrors used in previous resonator-based designs [18,19,28]. Furthermore, the 4f-stage allows for small incidence angles on the disk so that the angular spread between individual passes is small. The mirror array can thus be placed relatively far from the disk, in the telescope part of the resonator segment where the beam diameter is small, and 0.5" diameter array mirrors can be used. This minimizes astigmatism and reduces both cost and footprint of the multipass amplifier.

The 4f-stage also helps to mode match the input beam to the eigenmode of the multipass amplifier. The key idea is to measure the beam size on the unpumped disk versus effective focal power of the disk [23], where the distance between the focusing elements in the 4f-part is varied to tune ΔV according to (14) (see Fig. 8). In such plots, the beam size of a properly mode matched beam will show minimal oscillation around $\Delta V = 0$, i.e., around the nominal value of the focal length of the disk. Using this procedure, the disk cannot be pumped, since the soft aperture of the pump spot would suppress these oscillations [22,23]. In this data set, the beam size was measured after 6 passes over the disk as a compromise between sensitivity (sufficiently large oscillation signal) and time needed for alignment. In Fig. 8(a), the input beam is estimated to converge with half angle $\theta = 0.15$ mrad, which explains the relatively large oscillations in beam size [23]. In Fig. 8(b), the collimation of the input beam is optimized by slightly moving one of the telescope lenses used to mode match the input beam to the amplifier. The oscillations around $\delta_Y = 0$ mm are suppressed, meaning that the beam is correctly injected. The beam size is different in X (horizontal) and Y (vertical) directions because of a slight astigmatism, mainly introduced by the 4f-stage. Only minor adjustments of the amplifier are necessary when going from zero to full pump load. Our system is not only insensitive to changes ΔV of the disk focal power, but also exhibits high tolerance to misalignment of the disk. Indeed, with respect to disk

Optics EXPRESS

misalignment, our hybrid amplifier inherits the good stability properties of a purely FT-based amplifier which were discussed in [31].

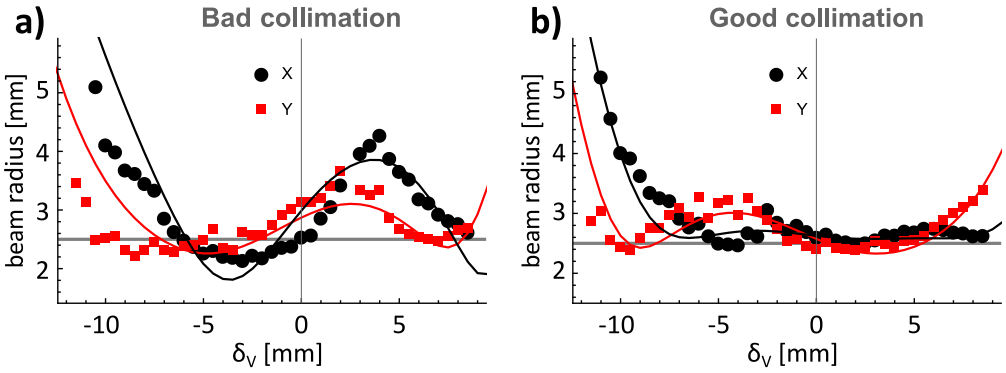

Fig. 8. Beam size at the disk on the 6th pass vs. effective focal power of the disk for the two transverse directions (X, Y). The effective dioptric power of the disk was scanned by varying δ_V, the separation between the imaging mirrors of the 4f-stage. The solid lines are fits with input beam diameter $w_0 = 2.75$ mm and beam divergence a) $\theta = 0.15$ mrad and b) $\theta = 0.126$ mrad (note that a "collimated" Gaussian beam has $\theta = \lambda/\pi w_0 \neq 0$).

5. Experimental results

For high-energy operation, the amplifier was setup to sustain a beam with $w_0 = 3$ mm at the disk. A small signal gain (i.e. small signal power amplification factor) of about 21 was measured with 20 passes (reflections) over the disk. For the small signal gain measurement, the oscillator was operated in CW, delivering a 150 mW beam to the amplifier. As shown in Fig. 9, the output beam was close to diffraction limited with $M^2 \leq 1.17$ in horizontal and vertical direction (measurement taken with Thorlabs BP209-IR2). The pump radiation is delivered by a volume Bragg grating stabilized diode stack running at 969 nm at the zero-phonon line of Yb:YAG. Compared to conventional pumping at 940 nm, the heat load is reduced by about 30 %, which further reduces thermal lensing effects in the amplifier. The pump spot had a diameter of $d_P = 8$ mm (full width half maximum, FWHM) and we limited the pump intensity to 2.5 kW/cm^2 to avoid overheating the 600 µm disk. At this pump intensity, the disk temperature did not exceed 100 °C. Interferometric measurements of the curvature of the disk yielded a thermally induced change in focal power of $\Delta V \lessapprox -0.015\,\mathrm{m}^{-1}$, which is well within the stability region shown in Fig. 3. The non-spherical deformation of the disk was not investigated in detail since the interplay between the FT propagation and the soft aperture formed by the pump spot suppresses non-spherical phase-front aberrations. The pump diameter was chosen based on the empiric law $d_P \approx 1.4 w_0$, often employed in the thin-disk laser community to ensure optimal energy transfer from a super-Gaussian pump spot to a TEM_{00} laser mode [22,32]. While in our case this law leads to $d_P \approx 8.4$ mm, the best results were obtained with a slightly smaller pump spot.

Seeded by pulses from our single-frequency TDL [27], the hybrid 20-pass amplifier delivered single frequency pulses of 50 ns and 100 ns length at 275 mJ and 330 mJ, respectively. The repetition rate was fixed to 100 Hz. To the best of our knowledge, this is the highest single frequency pulse energy obtained from a TDL to date. The amplifier gain was about 7 at 40 mJ input pulse energy for both pulse lengths. Figure 10 shows how the gain (dashed line) decreases as the extracted pulse energy increasingly depletes the inversion in the disk. The output energy E_{out} is fit with the Frantz-Nodvik equation [33]

$$E_{out} = E_{sat} \ln\left[1 + G_0\left(e^{E_{in}/E_{sat}} - 1\right)\right] \tag{15}$$

Optics EXPRESS

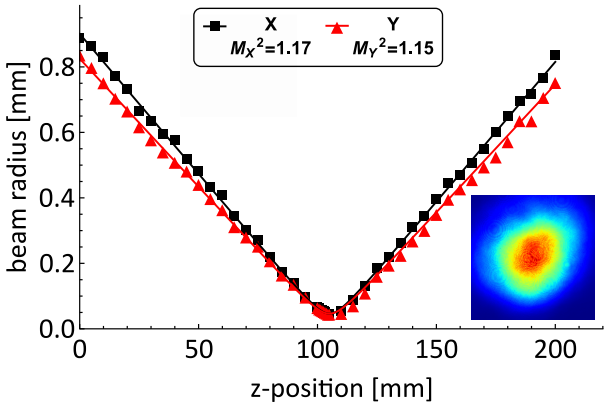

Fig. 9. M^2 measurement of the output beam of the 20-pass hybrid-type amplifier pumped at 2.5 kW/cm^2 and its beam profile.

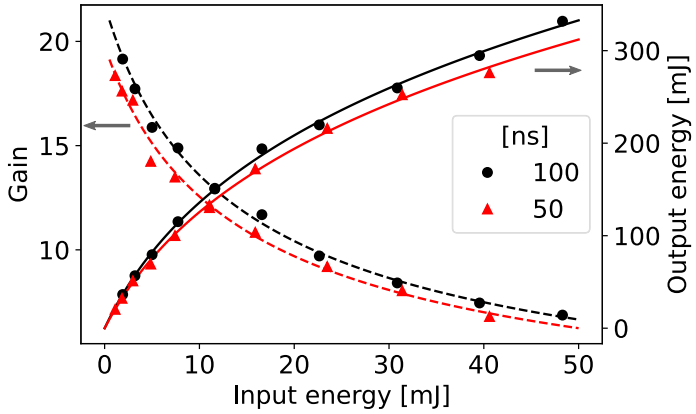

Fig. 10. Output pulse energy and gain (output energy divided by input energy) of the hybrid 20-pass amplifier versus input pulse energy for 100 ns and 50 ns long output pulses. The data is fit with the model given in Eq. (15). A gain of 6.9 is achieved for 100 ns pulses at an output pulse energy of 330 mJ. At around 275 mJ, optically induced breakdown of the air in the focus of the 4f-stage stared to take place for the 50 ns pulses. The small difference between the black and red curve is attributed to a slightly different alignment. The disk is 600 µm thick with 2.3 % doping, the beam size on the disk is w_0 = 3 mm and the pump intensity is 2.5 kW/cm^2 at 1300 W pump power.

where E_{in} is the input pulse energy, G_0 the small signal power amplification factor (which, for simplicity, we call the small signal gain), and E_{sat} the saturation energy. For the 100 ns pulses (black dots in Fig. 10), the fit resulted in $G_0 = 21.7$, agreeing well with the direct measurement of the small signal gain, and E_{sat} = 145 mJ. From E_{sat} the maximal extractable energy was calculated with

$$E_{\text{max}} = \lim_{E_{\text{in}} \to \infty} (E_{\text{out}} - E_{\text{in}}) = E_{\text{sat}} \ln G_0 \approx 445\,\text{mJ}. \tag{16}$$

The input pulse energy was not increased above 50 mJ to avoid laser-induced damage in the oscillator. For shorter pulses (50 ns at FWHM) the input energy was limited to around 275 mJ because above this threshold we observed the onset of laser induced ionization of the air, which prevented further energy scaling. This value agrees with laser induced breakdown of air,

Optics EXPRESS

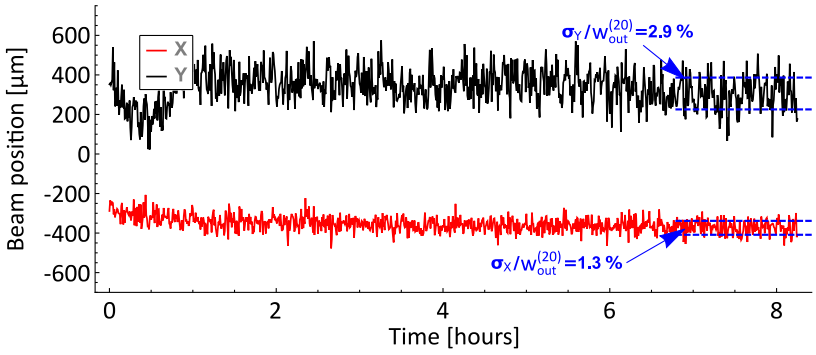

Fig. 11. Measured output beam position after 20 passes under full pump load and low-power CW operation. The jitter is about 2.9 % of the beam radius (2.75 mm) in the vertical (Y-direction) and about 1.3 % in the horizontal (X-direction).

assuming a diffraction limited spot size and basic scaling laws [34]. Given $E_{\max} \approx 445$ mJ, and the demonstration of the amplifier concept, we plan to reach the 500 mJ output energy level by increasing the pump intensity to 3.5 kW/cm^2, by slightly increasing the mode size on the disk and by increasing the waist at the focus of the 4f-stage.

After aligning the housed amplifier under full pump load, the system was continuously operated overnight, and showed only marginal misalignment over this period, as can be seen in Fig. 11. The pointing jitter was only <3 % and <1.5 % of the beam diameter (in this case 5.5 mm) in the vertical and horizontal direction, respectively, underlining the good stability against small misalignments of this amplifier. Thanks to the compact mirror array and the space saving 4f-propagation, the footprint of the multipass amplifier was about 1 m × 0.4 m, including the pump optics.

6. Discussion and conclusion

We demonstrated, for the first time, a compact hybrid multipass amplifier based on a succession of optical Fourier transform and 4f-relay imaging. While we realized a thin-disk amplifier with this architecture, the general scheme should be applicable to other laser types. Fourier transforming the beam in one part of the amplifier allows a passive compensation of phase front curvature errors and makes this amplifier suited for high-power applications where excellent beam quality is required. The 4f-stage in the other part of the amplifier is used to compensate shifts in focal length of the pumped disk and helps to mode match the injected beam. It also helps keeping the whole system compact. Moreover, changing the effective focal length of the disk by detuning the 4f-stage increases the flexibility of the system.

Currently the pulse energy is limited by the ionization of the air in the focus of the 4f-stage. This issue is readily solved by increasing the focal length of the mirrors used in the 4f-stage or by evacuating the region of the focus. The beam diameter in the FT part of the amplifier can easily be increased for example by increasing d_2 and using a larger f_{vex} to allow for further energy scaling. Larger mode sizes at the disk could require astigmatism compensation schemes, that could be implemented as in [30,35], by swapping the tangential and sagittal planes during propagation between the focusing mirrors of the 4f-stage.

Even though we developed an amplifier for laser spectroscopy of muonic atoms [25] that requires 100 ns pulses, we believe that the developed amplifier architecture has the potential to boost the energy of ultrashort pulses, as the beam size on all the optical components can be designed to be large while maintaining the stability properties of a stable resonator.

Optics EXPRESS

Funding. Partenariat Hubert Curien (Germaine de Stael 2023 projet No 48999PL); Schweizerischer Nationalfonds zur Förderung der Wissenschaftlichen Forschung (SNSF TMPFP2_210304); Agence Nationale de la Recherche (ANR-18-CE92-0030-02); Deutsche Forschungsgemeinschaft (EXC 1098 PRISMA (194673446), EXC PRISMA+ (390831469), LASIMUS (407008443)); Schweizerischer Nationalfonds zur Förderung der Wissenschaftlichen Forschung (SNF 200020_197052, SNF 200021_165854); European Research Council (CoG. #725039).

Acknowledgments. We gratefully acknowledge the support of the ETH Zürich electronics workshop. In particular, we thank Diogo Di Calafiori and Dr. Werner Lustermann. We also thank Dr. Marcos Gaspar, Dr. Carlo Vicario, Dr. Cezary Sidle and Stefan Mair from PSI.

Disclosures. The authors declare that there are no conflicts of interest related to this article.

Data availability. The data that support the findings of this study are available from the corresponding author upon reasonable request.

References

1. L. E. Zapata, H. Lin, A.-L. Calendron, *et al.*, "Cryogenic Yb:YAG composite-thin-disk for high energy and average power amplifiers," Opt. Lett. **40**(11), 2610–2613 (2015).
2. C. Herkommer, P. Krötz, R. Jung, *et al.*, "Ultrafast thin-disk multipass amplifier with 720 mJ operating at kilohertz repetition rate for applications in atmospheric research," Opt. Express **28**(20), 30164–30173 (2020).
3. S. Nagel, B. Metzger, D. Bauer, *et al.*, "Thin-disk laser system operating above 10 kW at near fundamental mode beam quality," Opt. Lett. **46**(5), 965–968 (2021).
4. R. Jung, J. Tümmler, and I. Will, "Regenerative thin-disk amplifier for 300 mj pulse energy," Opt. Express **24**(2), 883–887 (2016).
5. A. Loescher, F. Bienert, L. Pontagnier, *et al.*, "Thin-disk multipass amplifier delivering picosecond pulses with kW average power and highly-flexible intra-burst repetition: from MHz to multi-GHz," in *Advanced Solid State Lasers (ASSL 2023)*, (Tacoma, Washington, USA, 2023).
6. G. Račiukaitis, "Ultra-Short Pulse Lasers for Microfabrication: A Review," IEEE J. Sel. Top. Quantum Electron. **27**(6), 1–12 (2021).
7. M. Siebold, M. Loeser, F. Roeser, *et al.*, "High-energy, ceramic-disk Yb:LuAG laser amplifier," Opt. Express **20**(20), 21992 (2012).
8. Y. Ochi, K. Nagashima, M. Maruyama, *et al.*, "Effective Multi-pass Amplification System for Yb:YAG Thin-Disk Laser," in *Laser Congress 2017 (ASSL, LAC)*, (OSA, Nagoya, Aichi, 2017), p. JTh2A.31.
9. E. Perevezentsev, I. Kuznetsov, I. Mukhin, *et al.*, "Matrix multi-pass scheme disk amplifier," Appl. Opt. **56**(30), 8471 (2017).
10. D. N. Papadopoulos, F. Friebel, A. Pellegrina, *et al.*, "High Repetition Rate Yb:CaF_2 Multipass Amplifiers Operating in the 100-mJ Range," IEEE J. Sel. Top. Quantum Electron. **21**(1), 464–474 (2015).
11. M. Zwilich and B. Ewers, "Coherent beam combining of multipass thin-disk lasers with active phase control," OSA Continuum **3**(11), 3176–3186 (2020).
12. F. Druon, K. Genevrier, P. Georges, *et al.*, "Comparison of multi-pass and regenerative strategies for energetic high-gain amplifiers based on Yb:CaF_2," Opt. Lett. **45**(16), 4408 (2020).
13. S. Nagel, B. Metzger, T. Gottwald, *et al.*, "Thin disk laser operating in fundamental mode up to a power of 4 kW," in *The European Conference on Lasers and Electro-Optics*, (Optical Society of America, 2019), p. ca_5_4.
14. J.-P. Negel, A. Loescher, A. Voss, *et al.*, "Ultrafast thin-disk multipass laser amplifier delivering 1.4 kW (47 mJ, 1030 nm) average power converted to 820 W at 515 nm and 234 W at 343 nm," Opt. Express **23**(16), 21064 (2015).
15. M. Schulz, R. Riedel, A. Willner, *et al.*, "Pulsed operation of a high average power Yb:YAG thin-disk multipass amplifier," Opt. Express **20**(5), 5038 (2012).
16. T. Dietz, M. Jenne, D. Bauer, *et al.*, "Ultrafast thin-disk multi-pass amplifier system providing 19 kW of average output power and pulse energies in the 10 mJ range at 1 ps of pulse duration for glass-cleaving applications," Opt. Express **28**(8), 11415 (2020).
17. M. Hornung, H. Liebetrau, S. Keppler, *et al.*, "54 J pulses with 18 nm bandwidth from a diode-pumped chirped-pulse amplification laser system," Opt. Lett. **41**(22), 5413 (2016).
18. A. Antognini, K. Schuhmann, F. D. Amaro, *et al.*, "Thin-Disk Yb:YAG Oscillator-Amplifier Laser, ASE, and Effective Yb:YAG Lifetime," IEEE J. Quantum Electron. **45**(8), 993–1005 (2009).
19. K. Schuhmann, M. Ahmed, A. Antognini, *et al.*, "Thin-disk laser multi-pass amplifier," in *Solid State Lasers XXIV: Technology and Devices*, vol. 9342 (International Society for Optics and Photonics, 2015), p. 93420U.
20. M. Chyla, S. S. Nagisetty, P. Severová, *et al.*, "Generation of 1-J bursts with picosecond pulses from Perla B thin-disk laser system," in *Solid State Lasers XXVII: Technology and Devices*, W. A. Clarkson and R. K. Shori, eds. (SPIE, San Francisco, United States, 2018), p. 21.
21. A. Loescher, F. Bienert, C. Röcker, *et al.*, "Thin-disk multipass amplifier delivering sub-400 fs pulses with excellent beam quality at an average power of 1 kW," Opt. Continuum **1**(4), 747–758 (2022).
22. K. Schuhmann, K. Kirch, M. Marszalek, *et al.*, "Multipass amplifiers with self-compensation of the thermal lens," Appl. Opt. **57**(35), 10323 (2018).
23. M. Zeyen, "Thin-disk laser for the measurement of the hyperfine-splitting in muonic hydrogen," Ph.D. thesis, ETH Zurich (2021).

Optics EXPRESS

24. P. Amaro, A. Adamczak, M. A. Ahmed, *et al.*, "Laser excitation of the 1s-hyperfine transition in muonic hydrogen," SciPost Phys. **13**(2), 020 (2022).
25. J. Nuber, A. Adamczak, M. A. Ahmed, *et al.*, "Diffusion of muonic hydrogen in hydrogen gas and the measurement of the 1*s* hyperfine splitting of muonic hydrogen," SciPost Phys. Core **6**(3), 057 (2023).
26. M. Zeyen, L. Affolter, M. A. Ahmed, *et al.*, "Pound–Drever–Hall locking scheme free from Trojan operating points," Rev. Sci. Instrum. **94**(1), 013001 (2023).
27. M. Zeyen, L. Affolter, M. A. Ahmed, *et al.*, "Injection-seeded high-power Yb:YAG thin-disk laser stabilized by the Pound-Drever-Hall method," Opt. Express **31**(18), 29558–29572 (2023).
28. K. Schuhmann, "The Thin-Disk Laser for the 2S – 2P Measurement in Muonic Helium," Ph.D. thesis, ETH Zurich (2017).
29. J. Neuhaus, D. Bauer, J. Zhang, *et al.*, "Subpicosecond thin-disk laser oscillator with pulse energies of up to 25.9 microjoules by use of an active multipass geometry," Opt. Express **16**(25), 20530–20539 (2008).
30. J. Neuhaus, "Passively mode-locked Yb:YAG thin-disk laser with active multipass geometry," PhD Thesis, Universität Konstanz, Konstanz (2009).
31. K. Schuhmann, K. Kirch, A. Knecht, *et al.*, "Passive alignment stability and auto-alignment of multipass amplifiers based on Fourier transforms," Appl. Opt. **58**(11), 2904–2912 (2019).
32. M. Seidel, L. Lang, C. R. Phillips, *et al.*, "Influence of disk aberrations on high-power thin-disk laser cavities," Opt. Express **30**(22), 39691–39705 (2022).
33. L. M. Frantz and J. S. Nodvik, "Theory of Pulse Propagation in a Laser Amplifier," J. Appl. Phys. **34**(8), 2346–2349 (1963).
34. M. H. Niemz, "Threshold dependence of laser-induced optical breakdown on pulse duration," Appl. Phys. Lett. **66**(10), 1181–1183 (1995).
35. M. Larionov, F. Butze, D. Nickel, *et al.*, "Femtosecond thin disk Yb: KYW regenerative amplifier with astigmatism compensation," in *Advanced Solid-State Photonics*, (Optica Publishing Group, 2007), p. WB11.